**Harmful Algae**
December 2016, Volume 60 Pages 81-91
https://doi.org/10.1016/j.hal.2016.11.001
https://archimer.ifremer.fr/doc/00357/46858/



# Heterogeneous distribution in sediments and dispersal in waters of *Alexandrium minutum* in a semi-enclosed coastal ecosystem

Klouch Z. K. [1, 2], Caradec Florian [1], Plus Martin [1], Hernandez Farinas Tania [1, 2], Pineau-Guillou Lucia [3], Chapelle Annie [1], Schmitt Sophie [1], Quere Julien [1], Pineau-Guillou Lucia [2, 3], Siano Raffaele [1, *]

[1] IFREMER, DYNECO PELAGOS, Ctr Brest, F-29280 Plouzane, France.
[2] Sorbonne Univ, UPMC Univ Paris 6, Stn Biol Roscoff,CNRS, Adaptat & Diversite Milieu Marin UMR 7144,Equipe, Pl Georges Teissier,CS90074, F-29688 Roscoff, France.
[3] IFREMER, Ctr Brest, LOPS OC, F-29280 Plouzane, France.

* Corresponding author : Raffaele Siano, email address : raffaele.siano@ifremer.fr

**Abstract :**

Within the framework of research aimed at using genetic methods to evaluate harmful species distribution and their impact on coastal ecosystems, a portion of the ITS1rDNA of Alexandrium minutum was amplified by real-time PCR from DNA extracts of superficial (1–3 cm) sediments of 30 subtidal and intertidal stations of the Bay of Brest (Brittany, France), during the winters of 2013 and 2015. Cell germinations and rDNA amplifications of A. minutum were obtained for sediments of all sampled stations, demonstrating that the whole bay is currently contaminated by this toxic species. Coherent estimations of ITS1rDNA copy numbers were obtained for the two sampling cruises, supporting the hypothesis of regular accumulation of A. minutum resting stages in the south-eastern, more confined embayments of the study area, where fine-muddy sediments are also more abundant. Higher ITS1rDNA copy numbers were detected in sediments of areas where blooms have been seasonally detected since 2012. This result suggests that specific genetic material estimations in superficial sediments of the bay may be a proxy of the cyst banks of A. minutum. The simulation of particle trajectory analyses by a Lagrangian physical model showed that blooms occurring in the south-eastern part of the bay are disconnected from those of the north-eastern zone. The heterogeneous distribution of A. minutum inferred from both water and sediment suggests the existence of potential barriers for the dispersal of this species in the Bay of Brest and encourages finer analyses at the population level for this species within semi-enclosed coastal ecosystems.

**Graphical abstract**

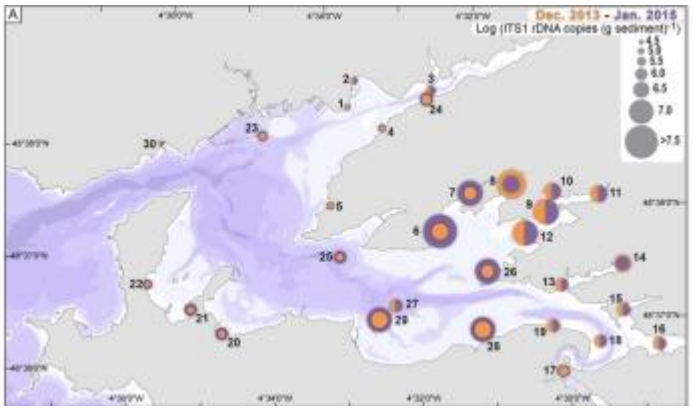


**Keywords** : Molecular ecology ; Dinoflagellate cyst ; Spatial distribution ; Real-time PCR ; Lagrangian model ; Population dynamics

## Introduction

The recovery of resting stages of harmful microalgae in sediment samples and the identification of accumulation sites indicate potential seeding sources for the initiation of blooms (Anderson et al., 2012). Cyst bank mapping is therefore particularly useful for the risk assessment of harmful microalgae, since it enables the prediction of blooming areas and the optimization of the management of coastal economic activities.

The distribution of *Alexandrium* species in coastal and shelf waters is relatively well known; however, comprehensive distributional data, especially for resting stage banks, are still needed (Anderson et al., 2012). On the basis of the available information, some common features in the distribution of *Alexandrium* cysts can be identified. Previous studies have reported that cyst accumulations are favored in fine-muddy rather than sandy sediments (White and Lewis, 1982, Kremp, 2000, Yamaguchi et al., 1996, Joyce et al., 2005, Gayoso et al., 2001, Matsuoka et al., 2003, Wang et al., 2004, Anderson et al., 2005, Anglès et al., 2010, Horner et al., 2011, Genovesi et al., 2013, Trikia et al., 2014, Fertouna-Bellakhal et al., 2015), supporting the hypothesis that dinoflagellate resting stages behave physically like fine particles (Dale, 1983). In semi-enclosed, confined ecosystems discrete cyst banks may be found (Anderson et al., 2012). A close link between the local distribution of cyst banks and blooms has been documented for some *Alexandrium* species in estuaries (Cembella et al., 1988, Crespo et al., 2011, Anderson et al., 2014), lagoons (Genovesi et al., 2009, Genovesi et al., 2013, Trikia et al., 2014, Fertouna-Bellakhal et al., 2015), and harbors (Bravo et al., 2008, Anglès et al. 2010). This local distribution has been associated with the hydrodynamic features of the studied ecosystems. Despite occurring in adjacent waters, local blooms of *A. fundyense* Balech were temporally separated, probably due to water retention in the first site where the blooms occurred (Crespo et al., 2011). Cyst densities of *A. tamarense* (Lebour) Balech were influenced by local hydrodynamics, with wind-induced currents causing cyst dispersal in the shallow ecosystem of the Thau lagoon (Genovesi et al., 2013). These examples prove the interest of

78 characterizing discrete, fine spatial scale cyst distributions to deduce local bloom dynamics in semi-
79 enclosed ecosystems.

80 Traditionally, hot spots of harmful microalgae accumulation in sediments are identified by
81 microscopy counting of their cysts (Genovesi et al., 2013), a method that is time-consuming and
82 suffers from taxonomical limitations in identification due to the lack of distinctive morphological
83 characteristics for the cysts of some species. In contrast, the analysis of specific genetic material in
84 sediment has proved to be a valuable alternative to infer cyst distribution, enabling a large number
85 of samples to be processed objectively in a relatively short time. The amplification of species-specific
86 marker genes from DNA preserved in sediment samples has been used to infer the presence of
87 dinoflagellate cysts (Godhe et al., 2002, Penna et al., 2010). Real-time PCR amplification to quantify
88 DNA genes from sediments has been shown to be a good proxy for cyst abundances, including some
89 *Alexandrium* species (Kamikawa et al., 2007, Erdner et al., 2010, Park and Park, 2010). Lastly, cyst
90 species have been mapped using the fluorescence in situ hybridization (FISH) technique (Hattenrath-
91 Lehmann et al., 2016). Genetic techniques can therefore be used to provide reliable information on
92 accumulation spots of cysts and to infer ecological patterns. Given the close association between
93 resting cyst abundance and sediment type, high specific DNA abundances should also be found in the
94 corresponding muddy sediments. The DNA extracted from sediments, however, can be of both
95 intercellular (resting stages) (Godhe et al., 2002, Erdner et al., 2010) and extracellular origin
96 (Pietramellara et al., 2009), making the relationship between specific DNA traces and sediment type
97 not completely predictable and still barely studied.

98 Although the analysis of genetic material in sediment cores showed that *A. minutum* Halim
99 has been present in the Bay of Brest since at least the 19th century (Klouch et al., 2016), the
100 vegetative form of the species was first identified within the framework of the REPHY (*REseau de*
101 *surveillance et d'observation du PHYtoplankton et des PHYcotoxine*s:
102 http://envlit.ifremer.fr/surveillance/phytoplancton_phycotoxines/presentation) in 1990. The first
103 cyst abundance survey was carried out in the same year and no cyst of *A. minutum* was found in four

104 estuarine stations of the Bay of Brest (Erard-Le Denn, 1993, Erard-Le Denn and Boulay, 1995). The
105 species abundance increased over time in the bay, reaching the record concentration of ca. 42 x $10^6$
106 cells $l^{-1}$ in July 2012 (Chapelle et al., 2015, Klouch et al., 2016) in the small, enclosed Daoulas estuary,
107 where bloom occurrences were unsuspected and monitoring was not carried out. In parallel, other
108 blooms of the species were observed in other estuaries on the bay (Elorn River, Aulne River), but
109 these were of minor importance (< 2 x $10^6$ cells $l^{-1}$). After the 2012 event, monitoring of Daoulas Bay
110 was initiated and seasonal blooms of *A. minutum* are observed in the Daoulas estuary along with
111 blooms of lower cell abundance in other monitored estuaries. The development of different
112 intensities in the Bay of Brest raises questions about the distribution of the major cyst banks of the
113 species and the potential connectivity between its different adjacent estuarine ecosystems.
114 In this study, both genetic analyses of sediments and model simulations in the water column
115 were used to try to explain the heterogeneity of *A. minutum* bloom occurrence in the Bay of Brest.
116 With a recently developed real-time PCR assay (Klouch et al., 2016), the ITS1rDNA copy number of *A.*
117 *minutum* from total DNA extracts of superficial sediments was quantified and used to infer the
118 distribution of cyst banks in the area. In parallel, the viability of these banks in the sampled stations
119 was determined in order to verify whether DNA genetic data correspond to viable resting stages of
120 the organisms and not only to the amplification of extracellular DNA. By means of a Lagrangian
121 physical model, passive particle trajectories released from different estuarine zones were simulated
122 in order to study the potential dispersal of *A. minutum* cells of different blooms and the connectivity
123 between different estuaries of the bay. The information gathered on both the benthic and the
124 pelagic habitat contributes to the understanding of *A. minutum* bloom dynamics in the Bay of Brest
125 and provides an example of heterogeneity in the dispersal of toxic microalgae in a semi-enclosed
126 coastal area.
127
128 **Materials and Methods**
129 *Study area*

130 The Bay of Brest (Brittany, France) is a semi-enclosed, marine ecosystem of 180 $km^2$ connected to the
131 Iroise Sea (Atlantic Ocean) by an opening 1.8 km wide and ~50 m deep (Fig. 1). The bay is a shallow
132 (about half of the total surface area is shallower than 5 m) macrotidal coastal system. The semi-
133 diurnal tidal amplitude ranges from 1.2 to 7.3 m (average of 4 m), leading to the presence of
134 extended intertidal flats during low tides. Frequent storms can induce a resuspension of material and
135 a very high turbidity (>100 mg $l^{-1}$ of sediments) over a long period of time (Hily et al., 1992). The bay
136 is characterized by fine and coarse sediments in shallow and deep waters, respectively, with a higher
137 proportion of muddy sediments in the upstream part of the estuaries (Hily et al., 1989). The
138 ecosystem hydrology is influenced by 5 different watersheds, with two main rivers, the Aulne (1842
139 $km^2$ catchment area, 30 $m^3$ $s^{-1}$ interannual mean flow) flowing into the south basin and the Elorn
140 (402 $km^2$ catchment area, 5.63 $m^3$ $s^{-1}$ interannual mean flow) flowing into the north basin,
141 contributing to about 80% of the total annual freshwater input. The total interannual mean flow has
142 stabilized after a four-decade rise, while the anthropogenic loads of nitrogen and phosphorous have
143 stabilized and decreased, respectively. The ban on washing powders containing orthophosphates in
144 the last two decades has resulted in a decreased phosphorous supply and thus a significant
145 imbalance in the N/P ratio (Chauvaud et al., 2000, Guillaud and Bouriel, 2007) which has led to
146 changes in the composition of planktonic and benthic communities (Quéguiner and Tréguer, 1984,
147 Del Amo et al., 1997, Chauvaud et al., 2000).
148
149 *Sampling strategy*
150 Thirty sites were selected in the Bay of Brest on the basis of available cartographies of sediment
151 typologies and benthic biotopes. Sampled stations correspond to ecosystems where: i) cyst
152 accumulation may be favored by the site geomorphology (estuaries, small bays with low flushing, low
153 bioturbation rates), ii) genetic material could be better preserved (muddy, anoxic sediments), iii)
154 human activities are developed and/or the impact of Harmful Algal Blooms is higher (harbors,
155 shellfish farming areas). Twenty-three stations were located in intertidal zones and seven in subtidal

areas (Table 1). Altogether, the 30 sampled stations cover well the geography of the Bay of Brest (Fig. 1). Samples were collected at low tide ± 2 hours during two campaigns of 3-5 days, both carried out during the winter of two consecutive years (December 2013 and January 2015). Subtidal stations were sampled by scuba divers. The top 3 cm of sediments was collected in triplicate using plastic syringes at 1-2 m distance from each other. Sediment samples were carefully preserved in different tubes. Samples of DNA were immediately frozen in liquid nitrogen then stored at -80°C in the laboratory while samples for cyst germination experiments were preserved in the dark at 4°C. Samples were preserved at 4°C for granulometry, at -80°C for chlorophyll *a* and pheopigments, and at -20° for organic carbon (OC).

*Sediment analyses*

Granulometry, chlorophyll *a*, pheopigment and organic carbon (OC) concentrations were determined from samples collected in triplicate at each station. Sediment grain size was analyzed using an LS 200 Beckman Coulter laser granulometer and sediment typologies were classified according to Larsonneur (1977) on the basis of four size classes (0-63, 63-125; 125-500; 500-2000 µm). For chlorophyll and pheopigment concentration measurements, sediment samples were freeze-dried just before extraction and analysis (Reuss and Conley, 2005). Before extraction, the sample was homogenized, and gravel and shell debris were removed. Chlorophyll *a* and pheopigments were extracted from 1 g of sediment with 10 ml of 90% acetone for at least 12 h at 4°C. Supernatants containing the extracted pigments were recovered after sample centrifugation. Chlorophyll *a* and pheopigment concentrations were determined spectrophotometrically at 750 and 665 nm before and after sample acidification with 0.3 N HCl (Lorenzen, 1967, Pusceddu et al., 2003). Sediment samples for OC measurement were ground and homogenized. Organic C was measured using a vario EL-III CNS elementary analyzer after decalcification of a subsample of the freeze-dried and ground sediment with phosphoric acid (Cauwet, 1975). Concentrations were calculated by comparison with

181 samples of known concentration of organic carbon (acetanilide, sulfanilamide) and analyses were
182 verified with a certified reference sediment sample.
183
184 *Molecular analyses*
185 Copy numbers of *A. minutum* ITS1rDNA were measured directly on DNA extracts from sediments
186 using a newly developed real-time qPCR assay (Klouch et al., 2016). Total DNA was extracted from 10
187 g of sediment material from each triplicate of all stations using the PowerMax soil isolation kit
188 (Mobio Laboratories Inc., Carlsbad, California, USA), following the manufacturer's instructions.
189 Extracts of DNA were eluted in a final volume of 5 ml and immediately stored at -80°C. Samples of
190 DNA were quantified by absorbance measurements using a Take3 trio microplate reader (BioTek,
191 Winooski, Vermont, USA) on 3 µl of DNA extract, and sterile water was used as the blank. The quality
192 of DNA was checked by 260/280 nm ratio to ensure that no contamination by proteins or other
193 components had occurred during DNA extraction.
194 Real-time PCR reactions were carried using primers Am_48F (5'-TGAGCTGTGGTGGGGTTCC-3') and
195 Am_148R (5'-GGTCATCAACACAGCAGCA-3') which target a fragment of 100 bp, the optimal amplicon
196 length for real-time PCR efficiency (Klouch et al., 2016). Prior to real-time PCR reactions, a standard
197 curve was constructed by cloning the ITS1rDNA gene from a local culture of *A. minutum* (A89) into a
198 plasmid (pCR 4) using a TOPO TA cloning kit (Invitrogen, USA). The standard curve was prepared with
199 10-fold serial dilutions of the plasmid containing the ITS1rDNA sequence of *A. minutum* and ranged
200 from $10^6$ to 10 copies $\mu l^{-1}$. Real-time PCR (quantitative PCR or qPCR) reactions were performed using
201 the iTaq Universal SYBR Green supermix kit (Bio-Rad) in a final volume of 20 µl. The reaction mixture
202 was composed of 10 µl of SYBR Green supermix (1X) containing (dNTPs, iTaq DNA polymerase,
203 MgCl2, SYBR Green I), 0.3 µM of the forward primer (Am_48F), 0.2 µM of the reverse primer
204 (Am_148R), sterile water and 2 µl of DNA template. The experiments were conducted in 96-well
205 plates containing the standard curve dilutions in duplicate, the target samples in triplicate and
206 negative controls composed of water instead of DNA in duplicate. The plates were loaded onto a

Stratagene Mxpro3000P (Agilent Technologies, Santa Clara, California, USA) thermal cycler with the following cycling conditions: 1 cycle at 95°C for 5 min followed by 40 cycles of 95°C for 5 sec and 62°C for 30 sec. A melting curve analysis was added at the end of each run to ensure specific *A. minutum* amplification. The optimal annealing temperature of 62°C was initially determined in conventional PCR. The primer combination that yielded the lowest threshold cycle value (Ct) and maximum real-time efficiency (Am_48F; 0.3 µM, Am_148R; 0.2 µM) was retained for further analysis. The reaction efficiency was estimated by the equation $E= 10^{(1/b)-1}$, where b is the slope of the standard curve. To ensure specific amplifications, the melting temperature values (Tm) were systematically checked by analyzing the melting curves. For further details, see Klouch et al. (2016). Abundances of *A. minutum* in each sample were expressed (assuming a 100% DNA extraction efficiency) in terms of copy number per g of wet sediment, using the following formula: Copy number x $g^{-1}$ = copy number $\mu l^{-1}$ x DNA extraction volume (µl)/sediment wet weight (g)

*Cyst germination experiments*

Germination experiments were carried out on samples from the 2013 series. An aliquot of ~5 $cm^3$ of sediment samples was added to filtered seawater and placed in an ultrasonic bath for 6 min to separate dinoflagellate cysts from inorganic particles. The 20-100 µm fraction of particles was retained for culturing experiments after sample sieving. Some drops of the 20-100 µm sediment fractions were distributed in 12-well plastic plates with K medium (Keller et al., 1987). The plates were placed in a culture room at 16°C, under an irradiance of 60 µmol photons $m^{-2}$ $s^{-1}$ and a light: dark cycle of 12 h:12 h. The plates were examined qualitatively once every day to check for *A. minutum* cell germination using an inverted microscope (Zeiss Axiovert 135). Germinated cells of *A. minutum* were identified using morphological characteristics (size, shape, plate arrangement).

*Simulation of* A. minutum *cell trajectories: Lagrangian transport*

The MARS3D hydrodynamic model (a detailed description is available in Lazure and Dumas, 2008) was used to study planktonic cell trajectories after bloom development. This numerical code solves

primitive physics equations (e.g. Navier-Stokes under hydrostaticity and Boussinesq assumptions) and is based on a finite difference scheme coupling barotropic and baroclinic modes within a sigma-coordinate framework. For this study, the model was defined for the Bay of Brest with spatial limits ranging between 48.203-48.447 °N and 4.093-4.730 °W, a spatial horizontal resolution of 50 meters and 20 vertical layers. Moreover, the model assumed a wetting and drying capability (intertidal areas), which is mass preserving. The model's bathymetry was provided by the SHOM (French Naval Hydrographic and Oceanographic Service). At its western and southern boundaries, the model was forced for water elevation (tides), water temperature and salinity by another model (Lazure et al., 2009), previously validated for tides and hydrology and simulating the Bay of Biscay and Channel hydrodynamics. Atmospheric forcing (wind and atmospheric pressure) came from the Météo-France AROME model (Seity et al., 2011) which has a temporal resolution of 1 hour and a spatial resolution of 0.025° (roughly 2.4 km). The three major rivers, the Aulne, the Elorn and the Mignonne, were taken into account, and water flows came from the HYDRO database (Governmental Environment Agency). Trajectories of *A. minutum* cells were computed by the ICHTYOP Lagrangian transport tool (Lett et al., 2008) coupled with the hydrodynamic model of the bay. This tool enables offline simulations of bloom dispersion by calculating fictive particle trajectories based on previously calculated currents. Two simulations were run for years 2014 and 2015. Particles were released at the beginning of June, when *Alexandrium* bloom conditions were fulfilled according to Chapelle et al. (2015), i.e. when the water temperature was above 15°C and during a neap tide period. Four different starting points were tested: stations 3, 9, 13 and 16 (Fig. 1). At each station, 1,000 passive particles were released in the surface layer within a square stain of 100 m side length. Each particle position was recorded during 10 days of simulations, which is the approximate period before particles are flushed out of the bay. The level of dropping (surface or bottom) was tested but had no significant influence on the results (not shown here). For these simulations, it was also assumed that particles had no buoyancy, no mortality and no growth and that they could not wash up on the coast. Connectivity between the four different release zones was assessed by defining reception areas as

the geographical limits of the four different estuarine areas: the Elorn estuary (incorporating station 3), the Daoulas estuary (incorporating station 9), the Camfrout estuary (incorporating station 13), and the Aulne estuary (incorporating station 16). Total numbers of particles released at each station and reaching the other three areas were computed. The model also enabled the calculation of the mean total distance covered by particles starting from the different stations as well as the total number of particles remaining in each area by the end of the simulation as a proxy for confinement.

*Statistical analyses*

A Principal Component Analysis (PCA) was used to assess relationships between environmental and biological data along a reduced number of axes (ade4 package for R; Dray and Dufour, 2007). Data used in the PCA included the four sediment size fractions (0-63 µm, 63-125 µm, 125-500 µm, 500-2000 µm) and the three biological variables (Chl *a*, *A. minutum* and total DNA concentration). To reduce the importance of observations with very high values, concentrations of *A. minutum* ITS1rDNA copy number $g^{-1}$ sediment were log10 (x+1)-transformed. The PCA result had the same dimension as the dataset, but the first principal components account as much as possible for the data variability. Thus, only the first two axes explaining most of the variance were retained for later interpretations. For graphical representation, PCA results were combined with a cluster analysis performed on environmental and biological variables (complete-linkage clustering, vegan package; Oksanen et al., 2015) to highlight further differences between station groups. A single cutting level (Euclidean distance = 8.2) was selected to obtain major groups of samples. Prior to these analyses, all variables were centered and scaled in order to make them dimensionally homogenous. Finally, the Spearman rank correlation coefficients were calculated between all the environmental and biological variables. All statistical analyses were performed using the R software (R Core Team, 2015).

**Results**

*Sediment analyses*

285 The relative magnitude of the granulometric size classes analyzed enabled each sampling site to be
286 classified on the basis of their sediment typology (Supp. Table 1) for the two sampling surveys. Of the
287 30 sampling stations, 13 were classified as sandy-mud, 6 as mud, 1 as muddy-sand, and 2 as fine
288 sand, coherently for both sampling surveys. For the remaining 8 stations, the granulometric
289 classification varied between the two years, more often due to variations in the percentage of either
290 or both 0-63 µm and 125-500 µm sediment size fractions.
291
292 *Quantification of* A. minutum *in DNA extracts of sediments*
293 Total DNA concentrations extracted from the sediments ranged from 1.95 to 55.20 ng $\mu L^{-1}$ for 2013
294 samples and from 1.57 to 36.08 ng $\mu L^{-1}$ for 2015 samples. According to 260/280 nm ratios, the DNA
295 extracts were of sufficient yield and purity to conduct amplification analyses. The reaction
296 efficiencies of real-time PCR amplifications of about 100 bp of the ITS1rDNA of *A. minutum* ranged
297 from 95 to 99% and the melting temperature values always corresponded to the expected value of
298 62°C, both results proving the high resolution of the PCR assay performed in this study. The ITS1rDNA
299 copy number varied from $1.63 \times 10^4$ to $5.46 \times 10^7$ copies $g^{-1}$ sediment in 2013 and from $2.89 \times 10^4$ to
300 $5.47 \times 10^7$ copies $g^{-1}$ sediment in 2015. Local *A. minutum* quantification was very variable between
301 replicates of some stations (the ranges of the standard errors between the three replicates were 3.57
302 $\times 10^4$ – $2.63 \times 10^7$ and $8.06 \times 10^4$ – $2.09 \times 10^7$ copies $g^{-1}$ sediment in 2013 and 2015, respectively)
303 showing a significant spatial variability for some stations at a very fine spatial scale (1-2 m) (Figs 2A,
304 B). At some stations, one replicate differed from the other two in one sampling year and not in
305 another (stations 1-10, 30), while for other stations the data between replicates were coherent for
306 the two years of analyses (stations 11-19). Stations 16-29 were characterized by higher copy
307 numbers in 2015 (Fig. 2B). Despite this strong intrasite variability, a coherent pattern of copy
308 numbers of ITS1rDNA of *A. minutum* was identified between the two years. On the whole, both the
309 intertidal (6-19) and subtidal (26-29) stations of the south-eastern part of the Bay of Brest were
310 characterized by higher copy numbers than the subtidal and intertidal stations of the western (20-22,

311 25, 30) and north-eastern part (1-5, 23-24) of the bay, in both 2013 and 2015. In particular, the
312 intertidal stations within Daoulas Bay (6-12) and the subtidal station outside the bay (26-29) were
313 characterized in both years by higher copy numbers of *A. minutum* ITS1rDNA (Fig. 2A).
314
315 *Germination experiments*
316 Germination of *A. minutum* occurred within the first 10 days of incubation of all (30/30) 2013
317 sediment samples. No differences (size, shape and swimming behavior) were observed in light
318 microscopy between specimens of different localities. In the light of the 2013 successful
319 germinations, cysts of the species were considered to have settled in all localities of the Bay of Brest
320 and therefore germination experiments were not performed on 2015 sediment samples.
321
322 *Genetic and environmental data correlations*
323 The PCA performed with genetic, sediment granulometry and biological environmental parameters
324 (Figs 3A, B) as well as Spearman correlations between variables (Fig. 3C) showed that *A. minutum*
325 ITS1rDNA copy numbers (labeled *A. minutum* DNA) and total DNA concentrations (labeled Total DNA)
326 were positively correlated with the fine sediment size fraction (labeled 0-63 µm),the Organic Carbon
327 (labeled OC),and chlorophyll *a* (labeled CHL *a*) concentrations (Figs. 3A, C). In particular, *A. minutum*
328 DNA was positively correlated with only fine sediment (0-63 µm) (0.54) and not with coarser
329 sediment types. The 0-63 µm sediment fraction and *A. minutum* DNA were both positively correlated
330 with OC concentration (0.60 and 0.83, respectively) (Fig. 3C). Cluster analysis identified two major
331 groups of stations (differentiated in dark (cluster 1) and light gray (cluster 2) in Fig. 3B). Overall, the
332 analysis separates the south-eastern intertidal and subtidal sampling stations of the Bay of Brest
333 (cluster 2: 6-12, 14-19, 26, 28, 29) where the highest percentages of the fine sediment size fraction
334 (0-63 µm) were associated with the highest concentrations of OC, CHL *a* and genetic material, from
335 the western and north-eastern stations (cluster 1: 1, 3-5, 20-22, 25, 30) where measured values of
336 these variables were lower. Yet, some exceptions to this geographical separation of sampling stations

were highlighted. Eastern stations 13 and 27 were characterized by low correlations and were grouped within cluster 1. On the contrary, the north-eastern station 24 was grouped within cluster 2, showing that the strong association between fine sediment granulometry, OC and CHL *a* and *A. minutum* copy number was not exclusive to a part of the Bay of Brest. Stations 2 and 23 had the same number of replicates in both clusters 1 and 2.

*Simulation of particle trajectories in the water*

Simulated trajectories and final particle positions after 10 days as a function of the initial release location and the year are shown in Figure 4 A-D as an example for 2015 (2014 simulated trajectories are not shown). Whichever year is considered, 56 to 81% of passive particles remain in the Bay of Brest after 10 days (Table 2). Particles released at Station 9 (Daoulas estuary) show the lowest percentage being flushed out of the Bay of Brest (Fig. 4B, Table 2), whilst particles released at station 3 (Elorn estuary) show the highest percentage (Fig. 4A, Table 2). The model simulations also show that particles released at stations 13 (Fig. 4C) and 16 (Fig. 4D) tend to be transported over greater distances than those released at stations 3 or 9. The Daoulas estuary appears to be the most confined area with 26.5-26.2% (depending on years) of the initial number of particles released at station 9 remaining in that area after 10 days (Table 2). The connectivity table between the four release areas (Table 3) shows similar patterns for 2014 and 2015 simulations. As expected, stations 13 and 16 show a high connectivity with the nearby Daoulas estuary (from 29.7 to 30.7% of the initial released particles). Interestingly, this connectivity seems to be rather one-way (from stations 13 or 16 towards the Daoulas estuary) since very few particles starting from station 9 (Daoulas estuary) reach the Camfrout estuary (0-0.4%) or the Aulne estuary (7.8-8.5%). The Daoulas and Elorn estuaries seem particularly hydrodynamically disconnected with very few particles released at station 9 reaching the Elorn estuary (0.2-0.3%) and similarly from station 3 to the Daoulas estuary (1.2-1.4% of particles). Moreover, after 10 days of simulation, no particle released from station 3 reaches the Camfrout estuary. In the center of the Bay of Brest, particles are well-mixed and come from each

363 releasing station. Overall, the simulations described here demonstrate that the south-east of the bay
364 is quite disconnected from the Elorn estuary, which is the area exporting the highest proportion of
365 particles outside the Bay of Brest, and that the Daoulas estuary is a confined area with little
366 connectivity with the Aulne estuary and even less with the Elorn estuary.
367
368 **Discussion**
369 *Genetic mapping of* A. minutum *in sediments*
370 In this study, a geographically exhaustive survey of the presence of *A.minutum* in superficial
371 sediment of the Bay of Brest (Brittany, France) during the winter of two consecutive years (December
372 2013 and January 2015) is provided. This is not the first screening of *A. minutum* traces in sediment
373 of the study area. In 1990, no cyst of *A. minutum* was found in four estuarine stations of the Bay of
374 Brest (Erard-Le Denn et al., 1993, Erard-Le Denn and Boulay, 1995) using cyst identification by light
375 microscopy. Here, real-time PCR amplification of a fragment of the ITS1rDNA of *A. minutum* from
376 DNA sediment extracts was proposed as an alternative method to cyst quantification. The high
377 proportion of extracellular DNA in the total environmental DNA extracts from sediments (Dell'Anno
378 and Danovaro, 2005) is an important issue to take into account when performing specific DNA
379 quantification in sediments. This problem may lead to misinterpreting the presence of viable material
380 (resting stages) in sediment and bias estimations of cyst abundances. Methods to separate
381 extracellular from intracellular DNA have been developed (Corinaldesi et al., 2005, Alawi et al., 2014,
382 Lever et al., 2015) but, even when this separation has not been directly applied, specific DNA
383 amplifications by PCR methodologies in field sediment samples have been shown to be a good proxy
384 of cyst abundances (Gohde et al., 2002, Erdner et al., 2010, Penna et al., 2010, Klouch et al., 2016),
385 most probably due to the better preservation of DNA material in resting stages (Boere et al., 2011).
386 The number of copies of genomic DNA markers and its variability among strains and growth phase
387 stages in dinoflagellates, including *Alexandrium* spp. (Galluzzi et al., 2010) and *A. minutum* in
388 particular (Galluzzi et al., 2004), may also cause a misinterpretation of the exact dinoflagellate cell

389 numbers in field samples when applying real-time PCR analyses. This issue has been discussed in
390 several studies focusing on the efficiency and limitations of the real-time PCR methodology (Gohde
391 et al., 2002, Gohde et al., 2008, Erdner et al., 2010, Galluzzi et al., 2010, Penna et al., 2010)
392 underlining the importance of taking into account this variability when monitoring HAB species. The
393 objective of this work was not to validate the real-time PCR amplifications to estimate exactly the
394 cyst abundances of *A. minutum*, but to map potential accumulation zones in the study area in order
395 to contribute to the understanding of the spatial heterogeneity of bloom dynamics and intensities of
396 *A. minutum* in the estuaries of the Bay of Brest.

397 Genetic traces of *A. minutum* were found in 30 out of 30 sampled stations of the study area.
398 In parallel, successful germination experiments of *A. minutum* on 2013 sediment samples proved that
399 living resting stages had settled in all stations and that the toxic species currently contaminates the
400 whole Bay of Brest. The reduced interstitial space between fine particles decreases water circulation
401 and can favor the establishment of anoxia in sediments, which are suitable conditions for slowing the
402 digenetic process and preserving organic matter (Genovesi et al., 2013). Therefore, as expected, the
403 organic matter content, chl *a* and total DNA concentrations were higher in stations characterized by
404 fine sand-muddy sediment typology, as proved for instance by the high correlation value (0.83)
405 obtained between the finest sediment fraction (0-63 µm) and the organic carbon content (Fig. 3). It is
406 acknowledged that *Alexandrium* cysts behave physically like fine particles and that accumulation
407 spots mostly occur in fine sediment areas (White and Lewis, 1982, Kremps, 2000, Yamaguchi et al.,
408 1996, Joyce et al., 2005, Gayoso et al., 2001, Matsuoka et al., 2003, Wang et al., 2004, Anderson et
409 al., 2005, Anglès et al., 2010, Horner et al., 2011, Genovesi et al., 2013). Consequently, DNA traces of
410 the species should mostly be found in sediments characterized by a large fraction of fine particles.
411 The good positive correlation found between the *A. minutum* ITS1rDNA amplifications and the 0-63
412 µm sediment fraction of the sampled stations confirms this hypothesis. Good correlations between
413 ITS1rDNA amplifications and the 0-63 µm sediment fraction were coherent for both 2013 and 2015
414 samples in stations of the south-eastern part of the Bay of Brest and particularly for stations of the

Daoulas estuary, in areas that were confirmed to be of muddy-fine sediment facies in a recent comprehensive, morpho-sedimentological analysis of the Bay of Brest (Gregoire et al., 2016).

Seasonal blooms of *A. minutum* have been detected in the Daoulas estuary since July 2012, when a massive toxic bloom event (concentrations of 42 x $10^6$ cells $l^{-1}$) highlighted the Daoulas area as a new risky zone for toxic blooms of *A. minutum* in the Bay of Brest (Chapelle et al., 2015). Before this event, the Daoulas area was not included in the monitored area of the REPHY observation network; in fact, the toxic species has only recently increased in the area as demonstrated by paleogenetic data from ancient sediment cores of the area (Klouch et al., 2016). As well as Daoulas Bay, blooms of the species occur in other zones of the Bay of Brest, but they have always been of minor intensity (Chapelle et al., 2015). In conclusion, large numbers of copies of the marker gene of *A. minutum* were found in sediments or areas where blooms of higher intensity occur in the plankton. This leads to the suggestion that the Daoulas estuary is probably an accumulation zone of cysts of *A. minutum* in the Bay of Brest, an area which should be carefully monitored for toxic bloom occurrences.

*Spatial heterogeneity in sediment and in water*

The mapping of the potential accumulation spots of *A. minutum* obtained for December 2013 and January 2015 suggests a non-homogenous distribution of cyst banks within the Bay of Brest, with major accumulation areas in the south-eastern part of the bay. In parallel, the simulation of passive particle trajectories performed with real forcings in potential offspring periods of *A. minutum* (June 2014 and 2015, the summer periods after the wintertime cyst accumulation in 2013 and 2015) suggests a differential dispersal of blooms in the bay. Blooms occurring in the south-eastern Daoulas estuary would be relatively disconnected from those in the north-eastern Elorn estuary, as the connectivity between the two areas is very low (<1.4%). The reasons for this heterogeneity in cyst banks and potential bloom dispersal must be found in the hydrology, geomorphology, and hydrodynamics of the bay.

441 Previous model simulations have shown that the estuaries of the Bay of Brest are preferential
442 ecosystems for dinoflagellate bloom occurrence because of a sustained nitrogen supply from rivers
443 (Menesguen et al., 2006) and significant estuarine nutrient stocks in sediment (Raimonet et al., 2013)
444 that can be resuspended (Tallberg et al., 2006) and due to low flushing rates in estuaries that allow
445 the development of the bloom (Sourisseau et al., accepted). Despite high nutrient loads, the Bay of
446 Brest seems to be resistant to eutrophication problems due to strong semi-diurnal tidal currents that
447 ensure the water exchange with the continental shelf (Le Pape and Menesguen, 1997, Chavaud et al.,
448 2000). In the shallow estuarine ecosystems of the Bay of Brest, the tide and the wind intensity and
449 direction could promote bottom currents that can influence cyst and sediment distributions as
450 shown in other semi-enclosed ecosystems (e.g. Genovesi et al., 2013, Trikia et al., 2014). Weak
451 bottom currents favor the settlement of fine-muddy (<0.63 µm) sediment and cysts of *Alexandrium*,
452 which are acknowledged to behave like fine sediment particles (Dale, 1983). Therefore, bottom
453 currents in the Bay of Brest may play a role in promoting the sediment movement and creating
454 permanent superficial deposits of *A. minutum* in the shallow, peripheral embayments of the south-
455 eastern zone of the bay, such as the Daoulas estuary. The specificity of the distribution pattern of *A.*
456 *minutum* in sediments of the Bay of Brest remains to be demonstrated. The cysts of different species
457 showed different abundance patterns in the same ecosystem (Park and Park, 2010, Satta et al., 2013,
458 Fertouna-Bellakhal et al., 2014). Therefore, the cysts of other dinoflagellate species might be
459 characterized by a different distribution in the Bay of Brest.
460 Sediment resuspension and transport in the water column of the Bay of Brest were analyzed
461 by hydro-sedimentary model simulations. Tide currents would generate higher concentrations of
462 resuspended muddy sediments in the south-eastern estuaries of the bay (the Daoulas and Aulne
463 estuaries) than in the north-eastern estuary (Elorn estuary) (Beudin et al., 2013, Beudin et al., 2014).
464 Tracked suspended mud of the south-eastern estuaries is predicted to be flushed out of the bay,
465 without reaching the Elorn estuary, while the mud of the Elorn estuary is expected to remain and
466 redeposit in the estuarine area without reaching the inner and south-eastern parts of the Bay of

Brest (Beudin et al., 2013, Beudin et al., 2014). In parallel, the simulated particle dispersal trajectories suggest tidal currents coupled with river outflows would trigger current trajectories that cause low exchanges between the north-eastern Elorn estuary and the south-eastern Daoulas, Camfrout and Aulne estuaries. Potential blooms developing in the Elorn estuary would be mostly directly exported out of the bay, whereas blooms developing in each of the south-eastern estuaries would be connected to each other but not to the Elorn estuary. Simulations of both sediment and particle transport suggest that the hydrodynamics of the bay would create barriers for *A. minutum* dispersal. Consequently, there could be low interbreeding between populations of the northern and southern zones of the Bay of Brest. The simulations carried out in this study are based on a physical model that does not include biological variables such as growth, asexual and sexual reproduction and mortality rates. These variables affect the retention time of a bloom and the connectivity between ecosystems and populations of the bay. New model simulations that integrate biological variables and a population genetic approach would complete the information provided by this study, probably supporting the heterogeneity of *A. minutum* dispersal in the Bay of Brest.

**Conclusions**

The successful germination of *A. minutum* from all sampled stations of the Bay of Brest demonstrates that *A. minutum* currently contaminates the whole Bay of Brest. Since in 1990 no cysts were found in estuarine samples of the bay, the information provided in this study contributes to highlighting a relatively recent proliferation of this toxic species in the bay. Higher copy numbers of ITS1rDNA in sediment samples of the Daoulas estuary argue in favor of the possibility that this estuary could be a major accumulation spot of the cysts of *A. minutum*. This distribution pattern could explain the regular occurrence of blooms of higher intensity in this area of the bay. The simulations of particle trajectories demonstrate that the blooms occurring in the north- and south-eastern estuaries of the bay are disconnected and therefore rather independent of each other. This suggests the existence of potential physical barriers to *A. minutum* bloom dispersal and of populations interbreeding in the

493 bay. Overall, a heterogeneous distribution of *A. minutum* in both sediment and the water column
494 emerge from this study, proving that there may be discrete, localized accumulations of cysts even in
495 a semi-enclosed coastal ecosystem.
496
497 **Acknowledgements**
498 This work was financed by the DAOULEX project supported by the Region Bretagne. This research
499 was carried out within the framework of K. Klouch's PhD funded by Ifremer and Region Bretagne
500 (Allocation de REcherche Doctorale (ARED) fellowship) and by the project of the ECosphere
501 Continentale et CÔtière (EC2CO) initiative of the Institut National des Sciences de l'Univers/Centre
502 National de la Recherche Scientifique (INSU/CNRS): PALMITO (2013-2015). The authors wish to thank
503 all colleagues who helped with sample collection and Xavier Caisey for scuba diving sampling
504 assistance. We wish to thank Dominique Hervio-Heath and members of the SG2M/LSEM laboratory
505 of Ifremer for access to their laboratory facilities and all their technical suggestions. Pierre Bodenes is
506 acknowledged for collaborating in the picture developments and Pascale Malestroit for helping with
507 culture maintenance. This research falls within the scope of the French GDR (Groupement de
508 Recherche) Phycotox (http://www.phycotox.fr) (2012-2018) on harmful microalgae and phycotoxins.
509
510 **References**
511 Alawi M., Schneider, B., Kallmeyer, J., 2014. A procedure for separate recovery of extra- and
512 intracellular DNA from a single marine sediment sample. J Microbiol Methods, 104, 36–42.
513
514 Anderson, D.M., Stock, C.A., Keafer, B.A., Nelson, A.B., Thompson, B., McGillicuddy, D.J. Jr., Keller,
515 M., Matrai, P.A., Martin, J., 2005. *Alexandrium fundyense* cyst dynamics in the Gulf of Maine. Deep-
516 Sea Res Pt II 52, 2522–2542.
517

518 Anderson, D.M., Alpermann, T.J., Cembella, A.D., Collos, Y., Masseret, E., Montresor, M., 2012. The
519 globally distributed genus *Alexandrium*: Multifaceted roles in marine ecosystems and impacts on
520 human health. Harmful Algae 14, 10-35.
521
522 Anderson, D.M., Keafer, B.A., Kleindinst, J.L, McGillicuddy, D.J. Jr., Martin, J.L., Norton, K., Pilskaln,
523 C.H., Smith, J.L., Sherwood, C.R., Butman, B., 2014. *Alexandrium fundyense* cysts in the Gulf of Maine:
524 long-term time series of abundance and distribution, and linkages to past and future blooms. Deep-
525 Sea Res Pt II 103, 6-26.
526
527 Anglès, S., Jordi, A., Garcés, E., Basterretxea, G., Palanques, A., 2005. *Alexandrium minutum* resting
528 cyst distribution dynamics in a confined site. Deep-Sea Res Pt II 57, 210–221.
529
530 Beudin, A., Chapalin, G., Guillou, N., 2013. Suspended sediment modeling in the Bay of Brest
531 impacted by the slipper limpet *Crepidula fornicata*. Proceedings of the 7th International Conference
532 on Coastal Dynamics, pp. 193-202.
533
534 Beudin, A., Chapalin, G., Guillou, N., 2014. Modelling dynamics and exchanges of fine sediments in
535 the Bay of Brest. La Houille Blanche 6, 47-53
536
537 Boere, A.C., Sinninghe Damsté, J.S., Rijpstra, W.I.C., Volkman, J.K., Coolen, M.J.L., 2011. Source-
538 specific variability in post-depositional DNA preservation with potential implications for DNA based
539 paleoecological records. Org Geochem 42, 1216-1225.
540
541 Bravo, I., Vila, M., Maso, M., Figueroa, R.I., Ramilo, I., 2008. *Alexandrium catenella* and *Alexandrium*
542 *minutum* blooms in the Mediterranean Sea: toward the identification of ecological niches. Harmful
543 Algae 7, 515-522.

544

545 Cauwet, G., 1975. Optimization of an analytical technique for evaluation of organic carbon in
546 sediments. Chem Geol 16, 59-63.

547

548 Cembella, A.D., Turgeon, J., Therriault, J.C., Beland, P., 1988 Spatial distribution of *Protogonyaulax*
549 *tamarensis* resting cysts in nearshore sediments along the north coast of the lower St. Lawrence
550 estuary. J Shellfish Res 7, 597–610.

551

552 Chapelle, A., Le Gac, M., Labry, C., Siano, R., Quéré, J., Caradec, F., Le Bec, C., Nézan, E., Doner, A.
553 Jeremie G., 2015. The Bay of Brest (France), a new risky site for toxic *Alexandrium minutum* blooms
554 and PSP shellfish contamination. Harmful Algae News, 51, 4-5.

555

556 Chauvaud, L., Jean, F., Ragueneau, O., Thouzeau, G., 2000. Long-term variation of the Bay of Brest
557 ecosystem: benthic-pelagic coupling revisited. Mar Ecol-Prog Ser 200, 35–48.

558

559 Corinaldesi, C., Barucca, M., Luna, G., Dell'Anno, A., 2011. Preservation, origin and genetic imprint of
560 extracellular DNA in permanently anoxic deep-see sediments. Mol Ecol 20, 642-654.

561

562 Crespo, B.G., Keafer, B.A., Ralston, D.K., Lind, H., Farber, D., Anderson, D.M., 2011. Dynamics of
563 *Alexandrium fundyense* blooms and shellfish toxicity in the Nauset Marsh System of Cape Cod
564 (Massachusetts, USA). Harmful Algae 12, 26-38.

565

566 Dale, B., 1983. Dinoflagellate resting cysts: benthic plankton. In: Fryxell, G.A. (Ed.), Survival Strategies
567 of the Algae, Cambridge University Press, Cambridge, pp. 69–136

568

569 Del Amo, Y., Quéguiner, B., Tréguer, P., Breton, H., Lampert, L., 1997. Impacts of high-nitrate
570 freshwater inputs on macrotidal ecosystems. II. Specific role of the silicic acid pump in the year-round
571 dominance of diatoms in the Bay of Brest (France). Mar Ecol Prog Ser 161, 225–237.
572 Dray, S., Dufour, A.B., 2007. The ade4 package: implementing the duality diagram for ecologists. J
573 Stat Softw 22, 1-20.
574
575 Dell'Anno, A., Danovaro, R., 2005. Extracellular DNA plays a key role in deep-sea ecosystem
576 functioning. Science 309, 2179.
577
578 Erard-Le Denn, E., Desbruyeres, E., Olu, K., 1993. *Alexandrium minutum*: resting cyst distribution in
579 the sediments collected along the Brittany coast, France. In: Smayda, T.J., Shimizu, Y. (Eds), Toxic
580 Phytoplankton in the Sea, Elsevier Science Publisher, Amsterdam, pp. 109–114
581
582 Erard-Le Denn, E., Boulay, V., 1995. Resting cysts of *Alexandrium minutum* in marine sediments:
583 quantification by three methods. In: Lassus, P., Arzul, G., Erard-Le Denn, E., Gentien, P., Marcaillou-Le
584 Baut, C. (Eds), Harmful Marine Algal Blooms, Lavoisier Publishing, Paris, pp. 257–730
585
586 Erdner, D.L., Percy, L., Keafer, B., Lewis, J., Anderson, D.M., 2010. A quantitative real-time PCR assay
587 for the identification and enumeration of *Alexandrium* cysts in marine sediments. Deep-Sea Res Pt II
588 57, 279–87.
589
590 Fertouna-Bellakhala, M., Dhib, A., Béjaoui, B., Turki, S., Aleya, L., 2014. Driving factors behind the
591 distribution of dinocyst composition and abundance in surface sediments in a western
592 Mediterranean coastal lagoon: report from a high resolution mapping study. Mar Pollut Bull 84, 347-
593 362.
594

595 Fertouna-Bellakhala, M., Dhib, A., Fathalli, A., Bellakhal, M., Chomérat, N., Masseret, E., Laabir, M.,
596 Turkic, S., Aleyaa, L., 2015. *Alexandrium pacificum* Litaker sp. nov (Group IV): Resting cyst distribution
597 and toxin profile of vegetative cells in Bizerte Lagoon (Tunisia, Southern Mediterranean Sea). Harmful
598 Algae 48, 69-82.

599 Galluzzi, L., Penna, A., Bertozzini, E., Vila, M., Garcés, E., Magnani, M., 2004. Development of a real-
600 time PCR assay for rapid detection and quantification of *Alexandrium minutum* (a dinoflagellate).
601 Appl Environ Microbiol 70, 1199–1206.

602 Galluzzi, L., Bertozzini, E., Penna, A., 2010. Analysis of rRNA gene content in the Mediterranean
603 dinoflagellate *Alexandrium catenella* and *Alexandrium taylorii*: implications for the quantitative real-
604 time PCR-based monitoring methods. J Appl Phycol 22, 1-9.

605 Gayoso, A.M., 2001. Observation on *Alexandrium tamarense* (Lebour) Balech and other dinoflagellate
606 population in Golfo Nuevo, Patagonia (Argentina). J Plankton Res 23, 463–468.
607
608 Genovesi, B., Laabir, M., Masseret, E., Collos, Y., Vaquer, A., Grzebyk, D., 2009. Dormancy and
609 germination features in resting cysts of *Alexandrium tamarense* species complex (Dinophyceae) can
610 facilitate bloom formation in a shallow lagoon (Thau, southern France). J Plankton Res 31, 1209–
611 1224.
612
613 Genovesi, G., Mouillot, D., Laugier, T., Fiandrino, A., Laabir, M., Vaquer A., Grzebyk D., 2013.
614 Influences of sedimentation and hydrodynamics on the spatial distribution of *Alexandrium*
615 *catenella/tamarense* resting cysts in a shellfish farming lagoon impacted by toxic blooms. Harmful
616 Algae 25, 15-25.
617

618 Gregoire, G., Ehrhold, A., Le Roy, P., Jouet, G., Garlan, T., 2016. Modern morpho-sedimentological
619 patterns in a tide-dominated estuary system: the Bay of Brest (west Brittany, France). J Maps.
620 http://doi.org/10.1080/17445647.2016.1139514
621
622 Godhe, A., Rehnstam-Holm, A.S., Karunasagar, I., Karunasagara, I., 2002. PCR detection of
623 dinoflagellate cysts in field sediment samples from tropic and temperate environments. Harmful
624 Algae 1, 361–73.
625
626 Gohde, A., Asplund, M.E., Hamstrom, K., Saravanan, V., Tyagi, A., Karunasagar, I., 2008.
627 Quantification of diatom and dinoflagellate biomasses in coastal marine seawater by real-time PCR.
628 Appl Environ Microbiol 74, 7174-7128.
629
630 Guillaud, J.-F., Bouriel, L., 2007. Relation concentration-débit et évolution temporelle du nitrate dans
631 25 rivières de la région Bretagne (France). RSE 20, 213.
632
633 Hattenrath-Lehmann, T.K., Zhen, Y., Wallace, R.B., Tang, Y.Z., Gobler, C.J., 2016. Mapping the
634 distribution of cysts from the toxic dinoflagellate *Cochlodinium polykrikoides* in bloom-prone
635 estuaries by a novel fluorescence *in situ* hybridization assay. Appl Environ Microb 82, 1114-1125.
636
637 Hily, C., 1989. La megafaune benthique des fonds meubles de la rade de Brest: pré-échantillonage
638 par vidéo sous-marine. Cah Biol Mar 30, 433-454.
639
640 Horner, R.A., Greengrove, C.L., Davies-Vollum, K.S., Gawel, J.E., Postel, J.R., Cox, A.M., 2011. Spatial
641 distribution of benthic cysts of *Alexandrium catenella* in surface sediments of Puget Sound,
642 Washington, USA. Harmful Algae 11, 96–105.
643

644 Joyce, L.B., Pitcher, G.C., du Randt A., Monteiro, P.M.S., 2005. Dinoflagellate cysts from surface
645 sediments of Saldanha Bay, South Africa: an indication of the potential risk of harmful algal blooms.
646 Harmful Algae 4, 309–318
647
648 Kamikawa, R., Nagai, S., Hosoi-Tanabe, S., Itakurab, S., Yamaguchi, M., Uchida, Y., Baba, T., Sakoa, Y.,
649 2007. Application of real-time PCR assay for detection and quantification of *Alexandrium tamarense*
650 and *Alexandrium catenella* cysts from marine sediments. Harmful Algae 6, 413–20.
651
652 Keller, M.D., Selvin, R.C, Claus, W., Guillard R.R.L., 1987. Media for the culture of oceanic
653 ultraphytoplankton. J Phycol 23, 633–38.
654
655 Klouch, Z.K., Schmidt, S., Andrieux-Loyer, F., Le Gac, M., Hervio-Heath, D., Qui-Minet, Z. N., Quéré, J.,
656 Bigeard, E., Guillou, L., Siano, R., 2016. Historical records from dated sediment cores reveal the
657 multidecadal dynamic of the toxic dinoflagellate *Alexandrium minutum* in the Bay of Brest (France).
658 FEMS Microbiol Ecol 92, http://doi.org/10.1093/femsec/fiw101
659
660 Kremp, A., 2000. Distribution, dynamics and *in situ* seeding potential of *Scrippsiella hangoei*
661 (Dinophyceae) cyst populations from the Baltic Sea. J Plankton Res 22, 2155–2169.
662
663 Larsonneur, C., 1977. La cartographie des dépôts meubles sur le plateau continental français:
664 methode mise au point et utilisée en Manche. J Rech Océanogr 2, 3439.
665
666 Lazure, P., Dumas, F., 2008. An external-internal mode coupling for a 3D hydrodynamical model for
667 applications at regional scale (MARS). Adv Water Resour 31, 233-250.
668

669 Lazure P., Garnier V., Dumas F., Herry, C., Chifflet, M., 2009. Development of a hydrodynamic model
670 of the Bay of Biscay. Validation of hydrology. Cont Shelf Res 29, 985-997.
671
672 Le Pape, O., Menesguen, A., 1997. Hydrodynamic prevention of eutrophication in the Bay of Brest
673 (France), a modelling approach, in: Ruddick, K. (Ed.) Processes in regions of freshwater influence
674 (PROFILE). J Marine Syst 12, 171-186
675
676 Lett, C., Verley, P., Mullon, C., Parada, C., Brochier, T., Penven, P., Blanke, B., 2008. A Lagrangian tool
677 for modelling ichthyoplankton dynamics. Environ Modell Softw 23, 1210-1214.
678
679 Lever, M.A., Torti, A., Eickenbusch, P., Michaud, A.B., Šantl-Temkiv, T., Jørgensen, B.B., 2015. A
680 modular method for the extraction of DNA and RNA, and the separation of DNA pools from diverse
681 environmental sample types. Front Microbiol 6, 476.
682 Lorenzen, C.J., 1967. Determination of chlorophyll and pheopigments: spectrophotometric
683 equations. Limnol Oceanogr 12, 343-346.
684
685 Matsuoka, K., Joyce, L.B., Kotani, Y., Matsuyama, Y., 2003. Modern dinoflagellate cysts in
686 hypertrophic coastal waters of Tokyo Bay, Japan. J Plankton Res 25, 1461–1470.
687
688 Menesguen, A., Cugier, P., Leblond, I., 2006. A new numerical technique for tracking chemical species
689 in a multisource, coastal ecosystem applied to nitrogen causing *Ulva* blooms in the Bay of Brest
690 (France). Limnol Oceanogr 51, 591-601.
691
692 Oksanen, J., Blanchet, G.F., Kindt, R., Legendre, P., Minchin, P.R., O'Hara, R.B., Simpson, G.L.,
693 Solymos, P., Stevens, M.H.H, Wagner, H., 2015. Vegan: Community Ecology Package. R package
694 version 2.3-0. http://CRAN.R-project.org/package=vegan.

695

696 Park, T.G., Park, Y.T., 2010. Detection of *Cochlodinium polykrikoides* and *Gymnodinium impudicum*
697 (Dinophyceae) in sediment samples from Korea using real-time PCR. Harmful Algae 9, 59-65.

698

699 Penna, A., Battocchi, C., Garcés, E., Anglès, S., Cucchiari, E., Totti, C., Kremp, A., Satta, C., Giacobbe,
700 M.G., Bravo, I., Bastianini, M., 2010. Detection of microalgal resting cysts in European coastal
701 sediments using a PCR-based assay. Deep-Sea Res Pt II 57, 288–300.

702

703 Pietramellara, G., Ascher, J., Borgogni, F., Ceccherini, M.T., Guerri, G., Nannipieri, P., 2009.
704 Extracellular DNA in soil and sediment: fate and ecological relevance. Biol Fert Soils 45, 219–35.

705

706 Pusceddu, A., Dell'Anno, A., Danovaro, R., Manini, E., Sara, G., Fabiano, M., 2003. Enzymatically
707 hydrolyzable protein and carbohydrate sedimentary pools as indicators of the trophic state of
708 detritus sink systems: A case study in a Mediterranean coastal lagoon. Estuaries 26, 641-650.

709

710 Quéguiner, B., Tréguer, P. (1984). Studies on the Phytoplankton in the Bay of Brest (Western Europe).
711 Seasonal variations in composition, biomass and production in relation to hydrological and chemical
712 features (1981—1982). Bot Mar 27, 449-460.

713

714 R Development Core Team. 2015. R: a Language and Environment for Statistical Computing. Vienna,
715 Austria. http://www.r-project.org/.

716

717 Raimonet, M., Andrieux-Loyer, F., Ragueneau, O., Michaud, E., Kerouel, R., Philippon, X., Nonent, M.,
718 Memery, L., 2013. Strong gradient of benthic biogeochemical processes along a macrotidal
719 temperate estuary: focus on P and Si cycles. Biogeochemistry 115, 399-417.

720

721 Reuss, N., Conley, D.J., 2005. Effects of sediment storage conditions on pigment analyses. Limnol
722 Oceanogr-Meth 3, 477-487.
723
724 Satta, C.T., Anglès, S., Lugliè, A., Guillén, J., Sechi, N., Camp, J., Garcés, E., 2013. Studies on
725 dinoflagellate cyst assemblages in two estuarine Mediterranean bays: a useful tool for the discovery
726 and mapping of harmful algal species. Harmful Algae 24, 65-79.
727
728 Seity, Y., Brousseau, P., Malardel, S., Hello, G., Bénard, P., Bouttier, F., Lac, C., Masson, V., 2011. The
729 AROME-France convective scale operational model. Mon Weather Rev 139, 976–991.
730
731 Sourisseau, M., Le Guennec, V., Le Gland, G., Plus, M., Chapelle, A., 2016. Understanding
732 phytoplankton's ecological niche and phenology using traits-based models applied to toxic algae.
733 Frontiers (accepted).
734
735 Tallberg, P., Tréguer, P., Beucher, C., Corvaisier, R., 2008. Potentially mobile pools of phosphorus and
736 silicon in sediment from the Bay of Brest: Interactions and implications for phosphorus dynamics.
737 Estuar Coast Shelf S 76, 85-94.
738
739 Trikia, H.Z., Daly-Yahiaa, O.K., Maloucheb, D., Komihaa, Y., Deidunc, A., Brahimd, M., Laabir, M.,
740 2014. Distribution of resting cysts of the potentially toxic dinoflagellate *Alexandrium*
741 *pseudogonyaulax* in recently-deposited sediment within Bizerte Lagoon (Mediterranean coast,
742 Tunisia). Mar Pollut Bulletin 84, 172-181.
743
744 Wang, Z., Qi, Y., Lu, S., Wang, Y., Matsuoka, K., 2004. Seasonal distribution of dinoflagellate resting
745 cyst in surface sediment from Changjang River Estuary. Phycol Res 52, 387–395.
746

White, A.W., Lewis, C.M., 1982. Resting cysts of the toxic red tide dinoflagellate *Gonyaulax excavata* in Bay of Fundy sediments. Can J of Fish Aquat Sci 39, 1185–1194.

Yamaguchi, M., Itakura, S., Nagasaki, K., Imai, I., Yasumoto, T., Oshima, Y., Fukuyo, Y. (Eds), 1996. Distribution and Abundance of Resting Cysts of the Toxic Dinoflagellates *Alexandrium tamarense* and *A. catenella* in sediments of the eastern Seto Inland Sea, Japan, Intergovernmental Oceanographic Commission of UNESCO, Laboratory of Bioorganic Chemistry, Tohoku University, Japan pp. 177–180.

## Table and Figure Legends

**Table 1.** List and coordinates of sampling stations. Subtidal stations (23-27) are indicated by a circle.

| Station ID | Station locality | Coordinates (N/W) |
|---|---|---|
| 1 | Polder | 48° 23' 3''/ 4° 26' 6'' |
| 2 | Moulin Blanc | 48° 23' 44''/ 4° 25' 55'' |
| 3 | Le passage | 48° 23' 25''/ 4° 23' 03'' |
| 4 | Kéraliou | 48° 22' 35''/ 4° 24' 41'' |
| 5 | Caro | 48° 20' 28''/ 4° 26' 26'' |
| 6 | Tinduff | 48° 20' 2''/ 4° 22' 03'' |
| 7 | Moulin Neuf | 48° 21' 5''/ 4° 21' 04'' |
| 8 | Penfoul | 48° 21' 25''/ 4° 19' 28'' |
| 9 | Kersanton | 48° 20' 45''/ 4° 18' 2'' |
| 10 | Lanveur | 48° 21' 19''/ 4° 17' 51'' |
| 11 | Rivière de Daoulas | 48° 21' 21''/ 4° 16' 2'' |
| 12 | Château | 48° 20' 11''/ 4° 18' 46'' |
| 13 | Moulin Mer | 48° 18' 56''/ 4° 17'11'' |
| 14 | Hôpital Camfrout | 48° 19' 37''/ 4° 14' 53'' |
| 15 | Tibidy | 48° 18' 25''/ 4°14' 40'' |
| 16 | Lanvoy | 48° 17' 47''/ 4° 13' 29'' |
| 17 | Térénez | 48° 16' 43''/ 4° 16' 49'' |
| 18 | Landévennec | 48° 17' 34''/ 4° 15' 29'' |
| 19 | Sillon des Anglais | 48° 17' 52''/ 4° 17' 22'' |
| 20 | Fret | 48° 16' 54''/ 4° 30' 13'' |
| 21 | Rostellec | 48° 17' 27''/ 4° 31' 30'' |
| 22 | Persuel | 48° 18' 1''/ 4° 33' 17'' |
| 23 o | Port de Commerce | 48° 22' 7''/ 4° 29' 18'' |
| 24 o | Le Passage | 48° 23' 39''/ 4° 22' 54'' |
| 25 o | Auberlac'h | 48° 19' 9''/ 4° 25' 53'' |
| 26 o | EstTinduff | 48° 19' 7''/ 4° 20' 7'' |
| 27 o | Lanveoc-Tinduff | 48° 18' 2''/ 4° 23' 31'' |
| 28 o | Quillien | 48° 17' 36''/ 4° 20' 6'' |
| 29 o | Ecole Navale | 48° 17' 37''/ 4° 24' 6'' |
| 30 | Sainte Anne | 48° 21' 41''/ 2° 33' 13'' |

**Table 2.** Summary of simulated particle trajectories initiating from four different areas in the Bay of Brest: F stands for the percentage of particles flushed out of the Bay of Brest at the end of the simulation, D is the mean cumulative distance covered by particles until the end of the simulation and A represents the percentage of particles still located in the estuary of release at the end of the simulation (auto-connectivity). The two numbers stand for years 2014 and 2015, respectively.

| Release station | 3 | 9 | 13 | 16 |
|---|---|---|---|---|
| *F* (%) | 43.6 – 37.7 | 9 – 18.7 | 29.1 – 30.8 | 23.5 – 24.2 |
| *D* (km) | 129.5 – 127.9 | 114.0 – 114.3 | 151.1 – 149.7 | 152.9 – 153.4 |
| *A* (%) | 9.4 – 8.3 | 26.5 – 26.2 | 0 – 0 | 12.8 – 10.4 |

**Table 3.** Connectivity table between releasing stations (3, 9, 13 and 16) and receiving areas (Elorn, Daoulas, Camfrout and Aulne estuaries). Percentage (%) of particles reaching the considered area at least once in 10 days for 2014 and 2015, respectively.

| | Releasing stations | | | |
|---|---|---|---|---|
| | St. 3 | St. 9 | St. 13 | St. 16 |
| Elorn estuary area | - | 0.3 – 0.2 | 1.6 – 2.0 | 2.0 – 0 |
| Daoulas estuary area | 1.4 – 1.2 | - | 29.7 – 28.4 | 30.7 – 28.0 |
| Camfrout estuary area | 0 – 0 | 0.4 – 0 | - | 6.6 – 6.0 |
| Aulne estuary area | 1.3 – 1.5 | 7.8 – 8.5 | 58.7 – 57.4 | - |

**Figure 1**. Map of the Bay of Brest indicating intertidal (stars) and subtidal (circles) sampling stations.

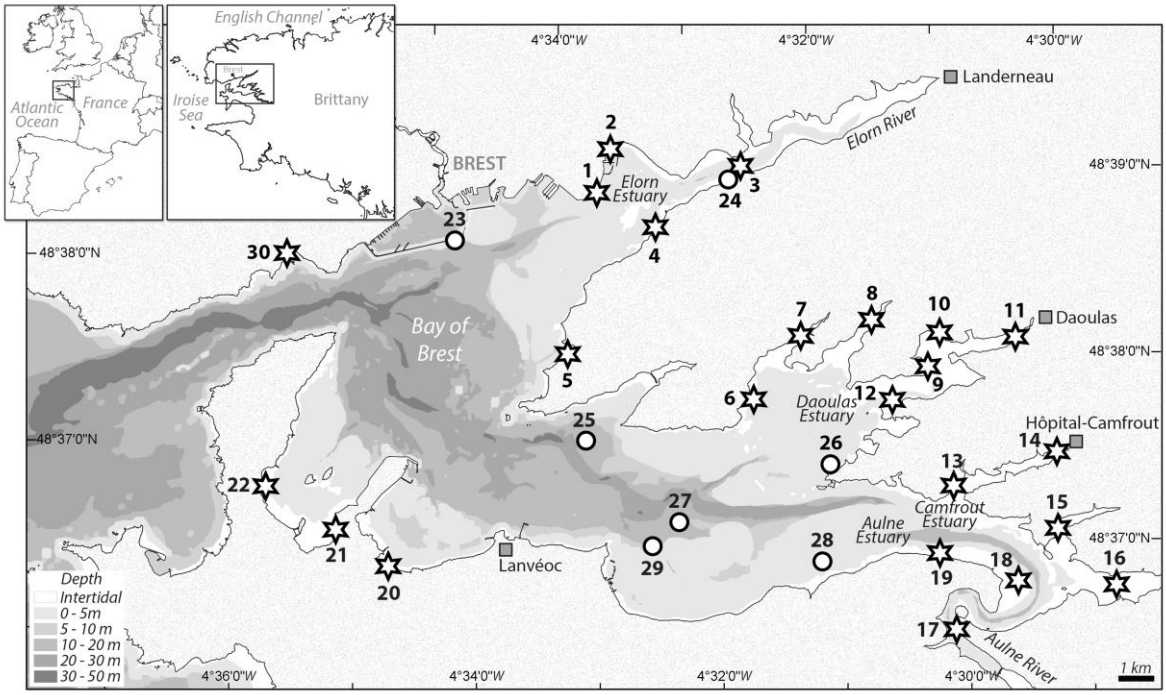

**Figure 2:** Log10 (x+1) transformed real-time PCR data of *Alexandrium minutum* copy number $g^{-1}$ of sediment at the 30 sampled stations during the two surveys (December 2013 and January 2015). A) At each station, colored circles represent the averaged values of copy number concentrations of the three replicates for each annual survey (yellow = December 2013; purple = January 2015). For each station, the highest concentration (larger circle) is in the background and the lowest is represented as a superposed circle. When the concentrations of the two years are of the same order of magnitude, each concentration value is represented by a semi-circle. B) Circles represent replicates for each sampling station and year. The dark gray bar represents the median of the six data values.

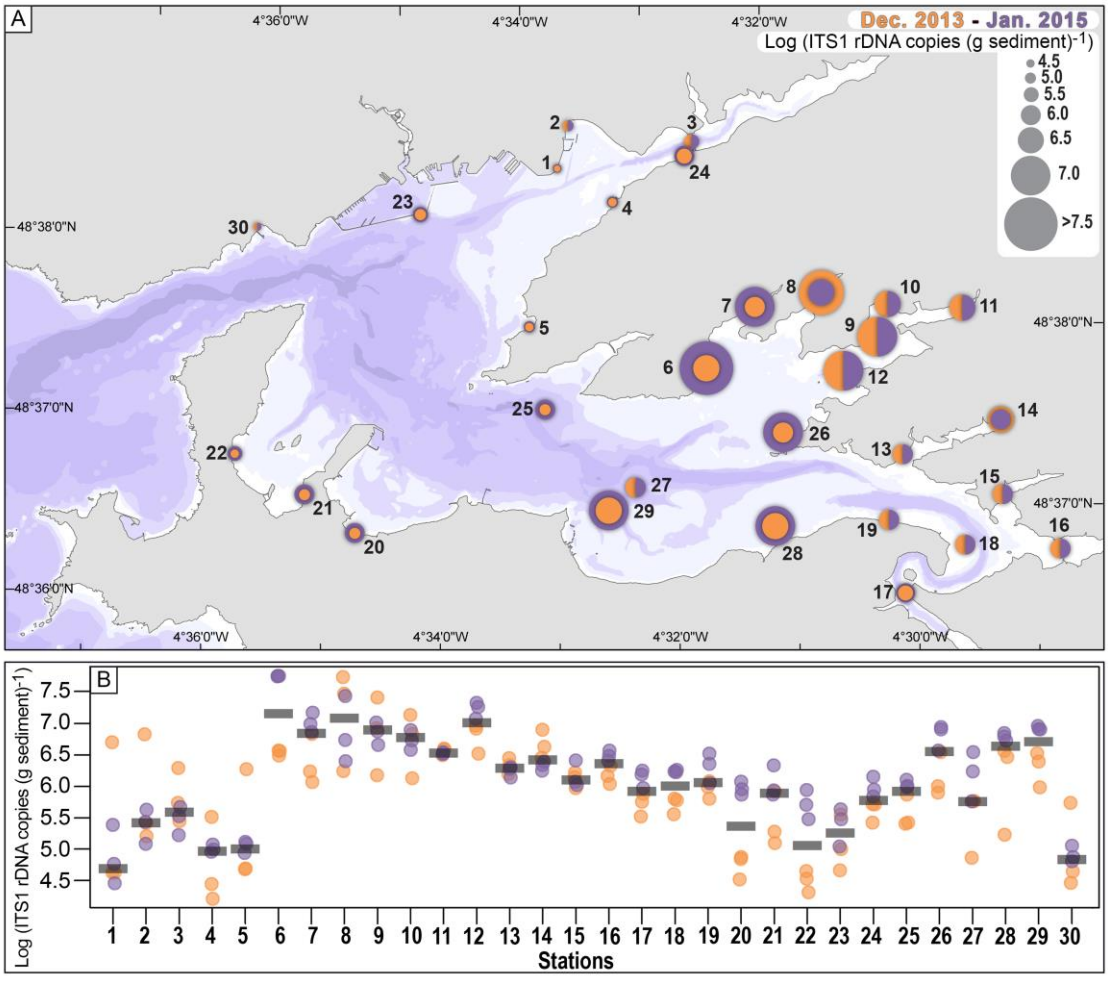

**Figure 3.** Relationship between environmental parameters (chlorophyll *a*: CHL *a*; organic carbon: OC, sediment size class: 0-63, 63-125, 125-500 and 500-200 µm), ITS1rDNA copy number concentration $g^{-1}$ of sediment of *Alexandrium minutum* (*A. minutum* DNA) and total DNA concentration (ng/µl) extracted from sediment (Total DNA). A) Projection of variables on the first two axes of the PCA accounting altogether for 69.37% of the total variance. B) Samples (site-year-replicate) scores with overlaid clustering results highlighting the two main sample groups detected by data clustering. Each circle represents a sample replicate; the color differentiates the sample clusters (cluster 1: dark gray and cluster 2: light gray): + symbol corresponds to the gravity center of each group of samples belonging to the same sampling station indicated by its corresponding number. (C) Spearman rank correlation coefficients between all variables. Light gray bars indicate positive correlations and dark gray bars negative correlations.

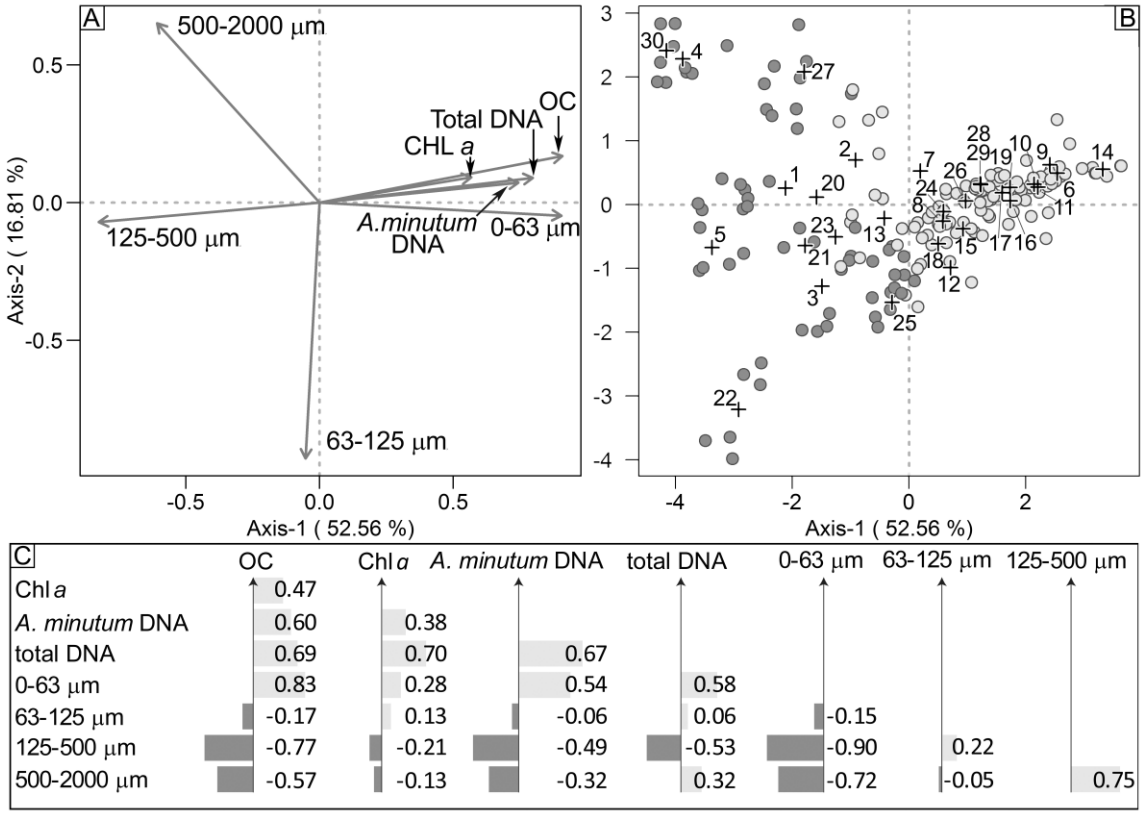

**Figure 4:** Simulated trajectories of 1000 passive particles coming from 4 releasing estuarine stations and reaching delimited estuarine areas: A) station 3 (Elorn estuary); B) station 9 (Daoulas estuary); C) station 13 (Camfrout estuary); D) station 16 (Aulne estuary). Simulation duration is 10 days and final particle positions are given as black dots.

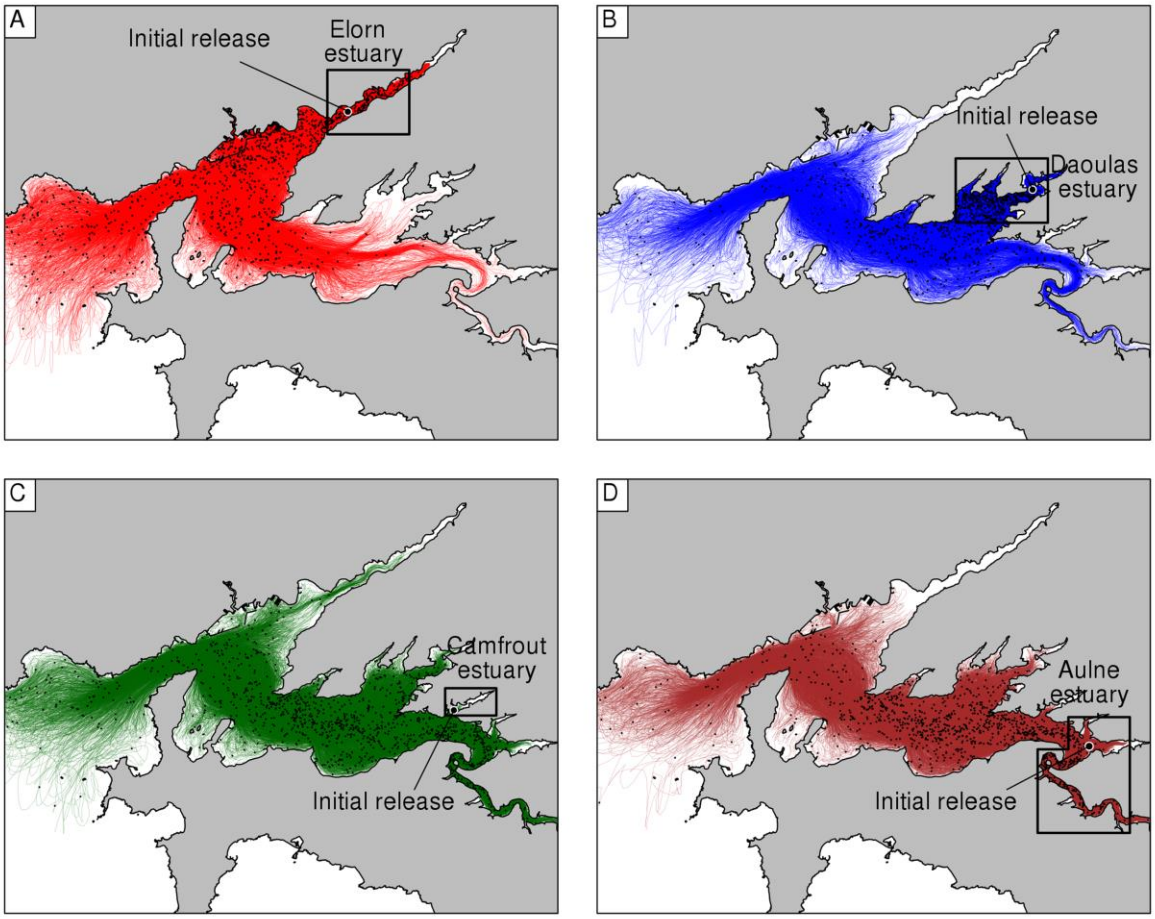

**Supp. Table 1.** Classification of sampling stations based on four sediment size classes (µm) following Larsonneur (1977) for the two sampling surveys (January 2013 and December 2015).

| Id St. | 0-63 | | 63-125 | | 125-500 | | 500-2000 | | Classification | |
|---|---|---|---|---|---|---|---|---|---|---|
| | *2013* | *2015* | 2013 | 2015 | 2013 | 2015 | 2013 | 2015 | 2013 | 2015 |
| 1 | *14.3 ± 7.7* | *53.8 ± 18.2* | 16.7 ± 0.9 | 11.9 ± 2.3 | 47.9 ± 9.4 | 20.4 ± 5.4 | 21.0 ± 2.7 | 13.9 ± 15.0 | Muddy sand | Sandy mud |
| 2 | *63.4 ± 4.7* | *27.4 ± 4.3* | 14.8 ± 0.6 | 12.0 ± 1.2 | 18.0 ± 2.9 | 24.7 ± 1.3 | 3.9 ± 2.5 | 35.9 ± 5.9 | Sandy mud | Sandy mud |
| 3 | *32.5 ± 0.6* | *40.8 ± 11.6* | 28.7 ± 0.3 | 18.1 ± 1.7 | 33.2 ± 0.9 | 33.6 ± 10.9 | 5.6 ± 0.5 | 7.5 ± 2.9 | Sandy mud | Sandy mud |
| 4 | *4.1 ± 0.7* | *5.5 ± 2.8* | 2.7 ± 0.5 | 2.2 ± 0.8 | 61.5 ± 1.5 | 55.0 ± 3.9 | 31.6 ± 2.3 | 37.3 ± 5.6 | Fine sand | Sandy mud |
| 5 | *3.6 ± 0.5* | *3.5 ± 0.6* | 17.3 ± 0.3 | 12.4 ± 4.6 | 75.6 ± 1.0 | 81.5 ± 5.3 | 3.4 ± 1.1 | 2.5 ± 0.7 | Fine sand | Fine sand |
| 6 | *81.9 ± 2.9* | *77.7 ± 5.5* | 11.2 ± 1.0 | 11.2 ± 1.6 | 6.3 ± 1.5 | 10.0 ± 4.0 | 0.6 ± 0.3 | 1.1 ± 0.3 | Mud | Mud |
| 7 | *69.6 ± 6.5* | *35.8 ± 6.6* | 16.0 ± 2.9 | 11.9 ± 0.2 | 12.4 ± 2.5 | 24.7 ± 4.2 | 2.0 ± 1.3 | 27.7 ± 9.9 | Sandy mud | Sandy mud |
| 8 | *61.2 ± 5.4* | *45.2 ± 6.3* | 18.9 ± 2.3 | 15.5 ± 2.1 | 17.6 ± 3.1 | 31.0 ± 2.4 | 2.2 ± 0.8 | 8.3 ± 3.6 | Sandy mud | Sandy mud |
| 9 | *62.6 ± 5.0* | *70.0 ± 6.4* | 11.9 ± 2.0 | 13.1 ± 1.0 | 18.9 ± 4.1 | 15.6 ± 4.7 | 6.5 ± 3.1 | 1.4 ± 1.3 | Sandy mud | Sandy mud |
| 10 | *76.0 ± 2.1* | *70.6 ± 2.2* | 12.4 ± 0.2 | 13.5 ± 0 | 9.8 ± 1.2 | 14.4 ± 1.7 | 1.8 ± 0.8 | 1.5 ± 0.6 | Mud | Sandy mud |
| 11 | *77.2 ± 1.1* | *76.5 ± 0.5* | 13.0 ± 0.4 | 12.8 ± 0.2 | 9.1 ± 0.6 | 9.9 ± 0.3 | 0.7 ± 0.2 | 0.8 ± 0 | Mud | Mud |
| 12 | *44.2 ± 3.2* | *52.5 ± 7.7* | 25.1 ± 3.3 | 22.2 ± 2.1 | 24.4 ± 1.6 | 22.2 ± 5.6 | 6.3 ± 2.0 | 3.0 ± 2.5 | Sandy mud | Sandy mud |
| 13 | *51.1 ± 11.1* | *36.7 ± 31.8* | 18.4 ± 1.8 | 12.7 ± 11.0 | 25.7 ± 9.5 | 15.1 ± 13.2 | 4.8 ± 3.2 | 2.2 ± 2.0 | Sandy mud | Sandy mud |
| 14 | *80.1 ± 1.4* | *74.1 ± 1.8* | 13.0 ± 0.5 | 13.5 ± 0.2 | 6.5 ± 1.0 | 11.6 ± 1.7 | 0.5 ± 0.2 | 0.9 ± 0.7 | Mud | Sandy mud |
| 15 | *69.6 ± 2.4* | *65.2 ± 3.5* | 16.5 ± 1.8 | 16.9 ± 1.2 | 12.2 ± 0.5 | 15.8 ± 2.0 | 1.6 ± 0.6 | 2.1 ± 0.8 | Sandy mud | Sandy mud |
| 16 | *70.0 ± 12.7* | *76.6 ± 0.4* | 16.2 ± 4.0 | 12.0 ± 0.5 | 12.4 ± 7.8 | 10.4 ± 0.6 | 1.4 ± 0.9 | 1.0 ± 0.3 | Sandy mud | Mud |
| 17 | *65.3 ± 6.1* | *64.2 ± 5.7* | 15.8 ± 1.0 | 13.5 ± 1.2 | 14.9 ± 2.9 | 18.6 ± 5.3 | 4.0 ± 2.7 | 3.6 ± 1.3 | Sandy mud | Sandy mud |
| 18 | *54.3 ± 8.5* | *70.0 ± 3.5* | 21.8 ± 1.6 | 15.6 ± 0.4 | 19.9 ± 6.9 | 12.9 ± 2.9 | 3.9 ± 3.2 | 1.5 ± 0.8 | Sandy mud | Sandy mud |
| 19 | *77.7 ± 2.3* | *82.1 ± 2.3* | 12.9 ± 0.4 | 10.8 ± 0.9 | 8.4 ± 1.5 | 6.8 ± 1.1 | 1.0 ± 0.4 | 0.3 ± 0.3 | Mud | Mud |
| 20 | *15.8 ± 7.8* | *67.4 ± 4.7* | 9.0 ± 2.0 | 17.5 ± 2.9 | 54.0 ± 11.1 | 14.1 ± 2.1 | 21.3 ±16.6 | 1.0 ± 0.3 | Muddy sand | Sandy mud |
| 21 | *49.8 ± 10.7* | *10.9 ± 0.9* | 23.7 ± 2.8 | 10.1 ± 0.5 | 23.9 ± 6.8 | 72.2 ± 0.8 | 2.5 ±1.1 | 6.8 ± 2.2 | Sandy mud | Muddy sand |
| 22 | *7.2 ± 1.1* | *10.4 ± 1.6* | 40.5 ± 1.8 | 31.9 ± 1.1 | 52.0 ± 2.7 | 56.5 ± 1.5 | 0.3 ± 0.1 | 1.2 ± 1.2 | Muddy sand | Muddy sand |
| 23 | *57.3 ± 6.8* | *27.5 ± 24.8* | 18.2 ± 1.1 | 12.4 ± 10.8 | 22.2 ± 3.8 | 23.3 ± 20.7 | 2.3 ±2.0 | 3.5 ± 4.5 | Sandy mud | Sandy mud |
| 24 | *69.1 ± 4.8* | *81.6 ± 1.1* | 15.9 ± 0.6 | 10.7 ± 1.0 | 12.9 ± 3.0 | 7.3 ± 0.2 | 2.1 ±1.4 | 0.3 ± 0.6 | Sandy mud | Mud |
| 25 | *63.3 ± 1.0* | *62.5 ± 1.5* | 24.9 ± 2.2 | 23.3 ± 1.6 | 10.4 ± 0.6 | 13.1 ± 0.6 | 1.4 ±1.1 | 1.1 ± 0.1 | Sandy mud | Sandy mud |
| 26 | *77.4 ± 3.3* | *81.5 ± 2.6* | 12.6 ±0.7 | 11.0 ± 1.5 | 9.4 ± 2.7 | 7.5 ± 1.2 | 0.6 ±0.1 | 0 | Mud | Mud |
| 27 | *35.1 ±2.8* | *32.1 ± 6.6* | 7.4 ±0.7 | 7.7 ± 1.4 | 19.4 ±2.1 | 25.9 ± 5.2 | 38.1 ±1.6 | 34.3 ± 10.5 | Sandy mud | Sandy mud |
| 28 | *77.7 ± 1.1* | *81.7 ± 4.0* | 10.4 ± 0.2 | 9.8 ± 1.2 | 11.1 ± 0.7 | 8.2 ± 2.3 | 0.9 ± 0.9 | 0.3 ± 0.6 | Mud | Mud |
| 29 | *79.4 ± 3.3* | *84.6 ± 0.7* | 10.9 ± 1.3 | 8.9 ± 0.4 | 8.9± 1.4 | 6.5 ± 0.6 | 0.8 ±0.7 | 0 | Mud | Mud |
| 30 | | *2.6 ± 1.3* | | 4.1 ± 0.9 | | 51.9 ± 6.2 | | 41.4 ± 7.3 | - | Fine sand |